ACS APPLIED MATERIALS & INTERFACES

Research Article

www.acsami.org

Fabrication of Carbon-Coated Silicon Nanowires and Their Application in Dye-Sensitized Solar Cells

Junhee Kim,[†] Jeongmin Lim,[‡] Minsoo Kim,[†] Hae-seok Lee,[†] Yongseok Jun,*[,‡] and Donghwan Kim*[,†]

[†]Department of Materials Science and Engineering, Korea University, Anam-dong, Seongbuk-gu, Seoul 137-713, Korea

[‡]Department of Materials Chemistry and Engineering, Konkuk University, Hwayang, Gwangjin, Seoul 143-701, Korea

Supporting Information

ABSTRACT: We report the fabrication of silicon/carbon core/shell nanowire arrays using a two-step process, involving electroless metal deposition and chemical vapor deposition. In general, foreign shell materials that sheath core materials change the inherent characteristics of the core materials. The carbon coating functionalized the silicon nanowire arrays, which subsequently showed electrocatalytic activities for the reduction of iodide/triiodide. This was verified by cyclic voltammetry and electrochemical impedance spectroscopy. We employed the carbon-coated silicon nanowire arrays in dye-sensitized solar cells as counter electrodes. We optimized the carbon shells to maximize the photovoltaic performance of the resulting devices, and subsequently, a peak power conversion efficiency of 9.22% was achieved.

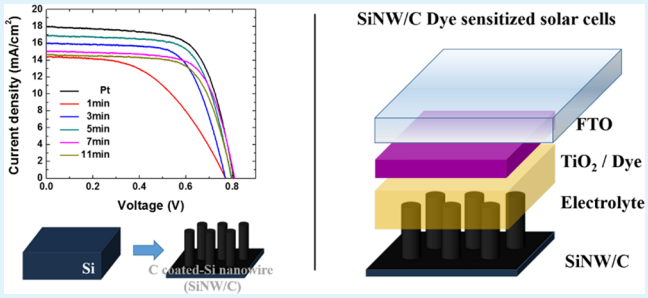

KEYWORDS: *silicon nanowire, core/shell nanostructure, carbon, counter electrode, dye-sensitized solar cells*

INTRODUCTION

One-dimensional (1D) nanostructured materials such as nanotubes and nanowires have emerged as promising building blocks in next-generation nanoscale devices such as photovoltaics,[1−3] photodetectors,[4−7] field effect transistors (FETs),[8−11] lithium ion batteries (LIBs),[12−14] and light-emitting diodes (LEDs).[15−17] In recent years, many researchers have investigated multifunctional core/shell nanostructured materials, whose multifunctional properties can be adjusted by the use of core materials sheathed by foreign shell materials. The 1D core/shell nanostructured materials have been used in diverse applications, and consequently, the devices based on such materials have shown improved performance and stability. Xia et al. reported the synthesis of unique porous core/shell nanowire array architectures, wherein the supercapacitor based on the core/shell nanoarrays showed enhanced performance.[18] Furthermore, Sun et al. reported the enhanced capability and cycling stability of lithium ion batteries based on $ZnCo_2O_4$/NiO core/shell nanowire arrays.[19]

The utilization of 1D core/shell nanostructured materials could also be expanded to electrocatalysts, which can be realized by sheathing core materials with foreign shell materials having electrocatalytic activity. Pt is a representative catalyst for the oxygen reduction reaction (ORR) in fuel cells and reduction of iodide/triiodide (I^-/I_3^-) in dye-sensitized solar cells (DSSCs). Although Pt counter electrodes have been considered to be the most efficient catalysts for the devices mentioned above, they need to be replaced by more earth abundant materials because Pt is required in many applications such as fuel cells and various catalysts. Therefore, much effort has been devoted to the investigation of Pt-free, carbon-based nanomaterials as catalysts, such as carbon black,[20] carbon nanotubes (CNTs),[21,22] and graphene.[23−25]

Even though many researchers have investigated 1D nanowire array-based photoelectrodes for DSSCs,[26−28] in this work, we synthesized carbon-coated silicon nanowires (SiNW/C) (i.e., silicon nanowire core/carbon shell) and employed them as counter electrodes in DSSCs. The defect rich carbon shells catalyzed the reduction of I^-/I_3^-. We obtained a maximal power conversion efficiency of 9.22%, which was comparable to that of the Pt counter electrode-based DSSCs (9.75%). To study the electrocatalytic performance in the reduction of I^-/I_3^- at the interface of the counter electrode, we conducted cyclic voltammetry (CV) and electrochemical impedance spectroscopy (EIS) analysis with the symmetric cell under AM 1.5G illumination. Although SiNW/C have been previously applied to LIBs as anodes,[29,30] to the best of our knowledge, this is the first report of their application to DSSCs.

EXPERIMENTAL SECTION

Synthesis of SiNW/C. Commercially available (100) n-Si wafer (0.001−0.003 Ω cm, Global wafer) was cut into pieces with dimensions of 1.5 cm × 1.5 cm. The Si pieces were ultrasonically cleaned with ethanol, acetone, and 2-propanol followed by a 30 min treatment in a UVO cleaner. The cleaned Si pieces were immersed in the etching solution containing 5 M HF and 0.02 M $AgNO_3$. After

Received: July 9, 2014
Accepted: October 16, 2014
Published: October 16, 2014

Scheme 1. SiNW Fabrication and Carbon Shell Deposition

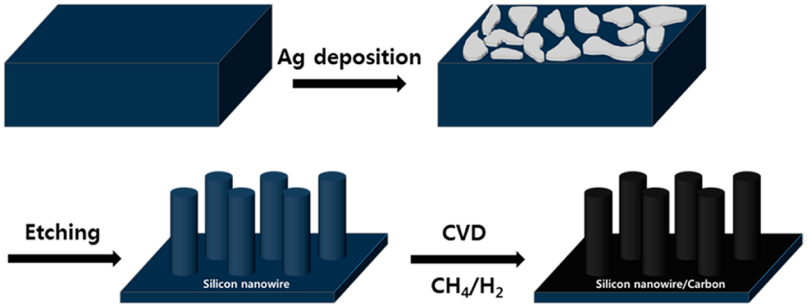

being etched for 30 min, the Si pieces were rinsed with deionized water and then immersed in a dilute HNO_3 solution for at least 30 min to remove Ag dendrites. A piece of a silicon nanowire (SiNW) array was located at the center of a tubular furnace. Once the temperature reached approximately 1075 °C, H_2 and CH_4 were simultaneously introduced into the reactor at flow rates of 100 and 100 sccm. The reaction time was controlled from 1 to 11 min.

Fabrication of DSSCs with Various Counter Electrodes. To clean the fluorine-doped tin oxide substrate (Nippon Sheet Glass Co., Ltd., Pilkington TEC Glass-TEC), it was sequentially washed with a detergent solution, deionized (DI) water, an ethanol/acetone mixture [1/1 (v/v)], and 2-propanol in an ultrasonic bath for 10 min. The substrate was subjected to UV−O_3 treatment for the duration of 15 min. Nanocrystalline TiO_2 paste (20 nm, ENB-Korea) was coated onto the cleaned FTO glasses using the doctor blading method. The TiO_2-coated FTO glasses were annealed at 500 °C for 1 h to create a TiO_2 film. After the heat treatment, the TiO_2-coated substrate was immersed in 0.3 mM $(Bu_4N)_2[Ru(dcbpyH)_2(NCS)_2]$ (termed N719) dye in a mixture of acetonitrile and *tert*-butanol [1/1 (v/v)] overnight at room temperature.

To prepare a Pt counter electrode in the DSSC, a 10 M H_2PtCl_6 solution in 2-propanol was coated onto a clean FTO glass, and the glass was annealed at 450 °C for 30 min. To prepare SiNW/C as the counter electrode in the DSSC, the as-prepared samples were used as is. A 50 μm thick Surlyn film (DuPont) was placed over the prepared electrode, and the counter electrode was subsequently placed. After the electrodes had been pressed at 100 °C for 3 s, the cell was sealed. The electrolyte solution containing a mixture of 0.5 M 4-*tert*-butylpyridine, 0.5 M 1-hexyl-2,3-dimethylimidazolium iodide, 0.05 M lithium iodide, and 0.02 M iodine in acetonitrile was introduced into the system, and a final sealing completed the fabrication of the cell (see Figure S1 of the Supporting Information).

Characterization and Measurements. The SiNW and SiNW/C were characterized using scanning electron microscopy (SEM) (Hitachi S-4300) and transmission electron microscopy (TEM) (JEOL, JEM-2100F) with instruments equipped with an X-ray energy dispersive spectrometer (EDS) to obtain information about micro- and nanostructures and compositions. The nanowires were mechanically detached by blading off the substrate and dispersed into ethanol, which was then dropped onto a lacey carbon TEM grid. A Raman spectrometer (LabRam ARAMIS IR2) equipped with a 532 nm diode laser was used to characterize the quality of the carbon shell on the SiNW. The photocurrent−voltage (J−V) curves of DSSCs were obtained using the current−voltage characteristic measurements under 100 mW/cm^2 AM 1.5G light (ABET Technology, LS 150 simulator). The photovoltaic performance was characterized using the V_{oc}, J_{sc}, fill factor (FF), and overall efficiency (η) values obtained from the J−V curve. Electrochemical impedance spectra (EIS) and cyclic voltammograms (CV) were measured using a symmetrically structured cell from the electrochemical station (Bio-Logic science instruments, VSP, CLB-2000).

RESULTS AND DISCUSSION

Scheme 1 illustrates the entire procedure from the SiNW fabrication to coating the SiNW surface with carbon. The SiNW were fabricated using an electroless metal deposition (EMD) method.[31] In brief, a piece of silicon wafer was etched in the etching solution of diluted HF and $AgNO_3$ at room temperature, followed by immersion in diluted HNO_3 to remove the excess Ag dendrites. Subsequently, carbon coating was performed using the chemical vapor deposition (CVD) process at 1075 °C for the desired reaction time with a mixture of CH_4 and H_2.

Figure 1a shows the cross-sectional morphology of the SiNW. The lengths and diameters of the SiNW are ∼17 μm and in the range of 220−500 nm, respectively. Panels b and c show the tilted top images of the SiNW and SiNW/C, respectively. Compared to the bare SiNW (not coated with carbon) with sharp tips, the SiNW/C have smooth tips. Bare SiNW tips were highly congregated, and this might be caused by the mutual attraction between dangling bonds and electrostatic charges present on the surfaces of the SiNW.[32] The mutual attraction was released a bit once the surface was covered with carbon as shown in Figure 1b.

Figure 2 shows the TEM images of samples obtained at different reaction times. Figure 2a shows the low-magnification image of a single nanowire after carbon coating (3 min), while panels b−f show the high-resolution images of the representative samples corresponding to 1, 3, 5, 7, and 11 min, respectively. The X-ray energy dispersive analysis (EDS) reveals the presence of the carbon shell on the surface of silicon after reaction for 5 min, as shown in Figure S2 of the Supporting Information. According to the data, we can observe C and Si as main peaks, while the intensity for O is quite small (only 2.51 atomic weight percent). The carbon thickness around the SiNW tended to gradually increase with an increasing reaction time from 1 to 11 min as follows: 0.7, 9, 17, 19, and 26 nm. The increase in the surface area was observed for the first 5 min, and then the surface area decreased.[33]

The quality of the carbon shell and the degree of defects were investigated using Raman spectroscopy by examining intensity ratios (I_D/I_G) of D and G peaks (Figure 3). A 521 cm^{-1} peak originated from the Si−Si vibrational mode,[34] and peaks at around 1350 and 1600 cm^{-1} corresponded to the disordered (D band) and graphitic (G band) bands from the carbon shell, respectively. As the reaction time increased, the relative intensity of the D and G peaks increased with respect to that of the silicon peak. The I_D/I_G ratio obtained from the sample after a reaction time of 1 min was the lowest (1.2), beyond which it remained almost constant (1.4−1.5). The relatively low I_D/I_G ratio of the sample reacted for 1 min probably originated from the thin carbon shell.[35] The peak positions of D and G bands and the I_D/I_G ratios are summarized in Table 1. These I_D/I_G ratios are quite

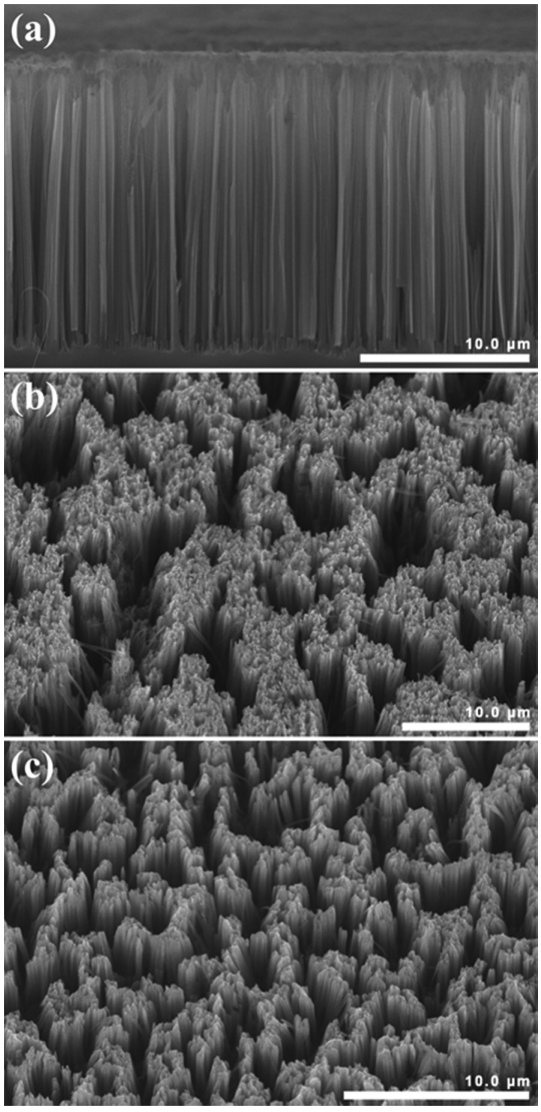

Figure 1. SEM images of vertically aligned as-prepared SiNW array (a), tilted SiNW (b), and SiNW/C (c).

comparable to those published elsewhere.[36−38] For instances, Cruz et al. prepared a transparent graphene-based counter electrode and obtained up to 7.5% with a value of 1.15,[37] and Akbar et al. introduced FTO-free counter electrodes for DSSCs using carbon nanosheets with values of 1.04−1.41 and a maximal performance of ∼5%.[38]

To examine the interfacial electrochemical properties with the amount of deposited carbon, EIS was employed. Figure 4 shows the Nyquist plot of the symmetrical cells (often called dummy cells) with coating times of 1, 3, 5, 7, and 11 min, and a conventional Pt-coated electrode. The first semicircle at the high frequency was ascribed to the charge transfer at the interface between the electrode of interest and electrolyte, while the second semicircle at the low frequency was associated mainly with the Nernst diffusion of I_3^- within the electrolyte. At the SiNW/C counter electrode, the charge transfer resistance (R_{ct}) value was directly related to the number of catalytic sites.[39−44] For this reason, a sample with a 1 min carbon coating showed the largest internal resistance because of the small amount of catalytic carbon coating, as seen in the inset of Figure 4. Because the higher carbon contents could provide more catalytic sites for the reduction of I_3^-, we observed that

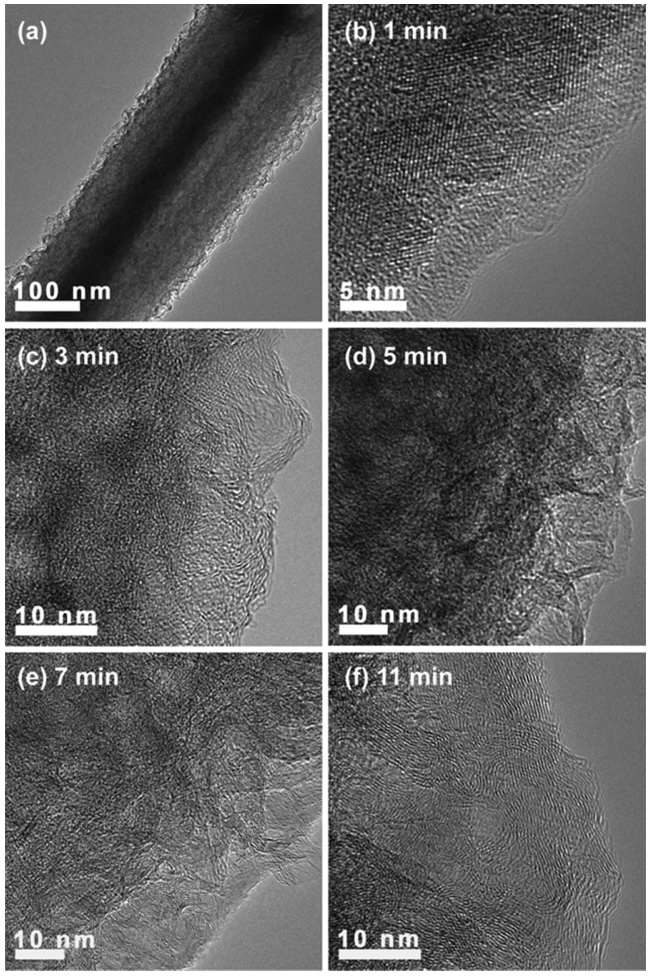

Figure 2. (a) Low-magnification TEM image of a single SiNW/C and (b−f), HRTEM images of carbon shells deposited on the SiNW surface at different reaction times: 1, 3, 5, 7, and 11 min, respectively.

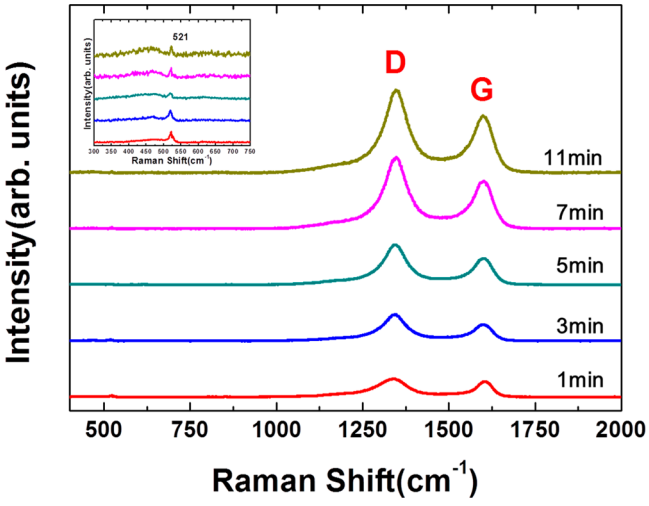

Figure 3. Raman spectra of SiNW/C obtained under different reaction times. D and G peaks of carbon shells were plotted with respect to the silicon peak (inset).

the R_{ct} value of a sample with a 5 min carbon coating was the lowest among the samples. The samples with 9 and 11 min carbon coatings showed even longer times for carbon deposition. However, the surface area decreased with over-

Table 1. Peak Positions of G and D Bands and I_D/I_G Ratios

	D band (cm^{-1})	G band (cm^{-1})	I_D/I_G
1 min	1344	1600	1.2
3 min	1344	1600	1.5
5 min	1343	1600	1.5
7 min	1346	1600	1.5
11 min	1345	1600	1.4

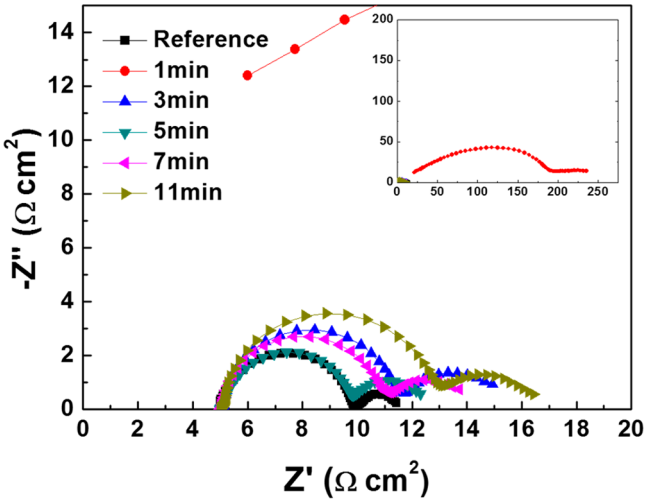

Figure 4. Nyquist plots from electrochemical impedance spectroscopy with symmetrical counter electrodes.

reaction and could not yield smaller R_{ct} values compared to the sample with a 5 min carbon coating. The low-frequency semicircle, which was related to electrolyte diffusion, had similar shapes for all the samples because the diffusion in the electrolyte was indifferent to the catalytic activity of the counter electrodes.

The equivalent circuit of this type of cell (symmetrical cell) is described in the inset of Figure 5. R_{sheet}, R_{ct}, and R_d represent

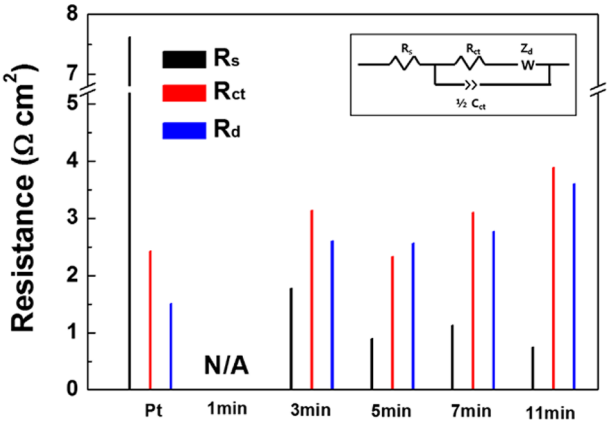

Figure 5. Calculated series resistances, charge transfer resistances, and diffusion resistances of different counter electrodes.

series resistance in the high-frequency region, charge transfer resistance, and Warburg diffusion, respectively. Using the simulating system (Solartron), the R_{sheet} and R_{ct} values were analyzed and are shown in Figure 5 and Table 2.

Because the conductance of the silicon substrate is higher than that of FTO, R_{sheet} values for Si-based samples were lower than those of FTO-based samples. However, R_{ct} values show

Table 2. Calculated Values of Series Resistances, Charge Transfer Resistances, and Diffusion Resistances with Different Counter Electrodes

counter electrode	R_{sheet} (Ω cm^2)	R_{ct} (Ω cm^2)	R_d (Ω cm^2)
Pt	7.62	2.43	1.51
1 min	N/A	N/A	N/A
3 min	1.78	3.14	2.6
5 min	0.89	2.33	2.56
7 min	1.13	2.9	2.77
11 min	0.75	3.89	3.6

the other trend because Pt exhibits the best performance as summarized in Table 2, and these values are well matched to previously reported values.[45]

As shown in Figure 5, R_{ct} values of samples treated for 3 and 5 min is gradually decreased, whereas R_{ct} values for samples treated for 7 and 11 min are increasing. This trend has been discussed with previous photocurrent explanation. Because R_{ct} is directly related to the number of active catalytic sites, the reaction time of 5 min may give the highest number of active sites exposed to an electrolyte. After the time, extra carbons may close the porosity of the surface; therefore, they do not play important roles in increasing active catalytic sites. EIS data for full cell are shown in Figure S3 of the Supporting Information with a brief description.

To elucidate the electrochemical properties, CV analyses (additional information in Figure S4 of the Supporting Information) were employed. Figure 6 represents the electro-

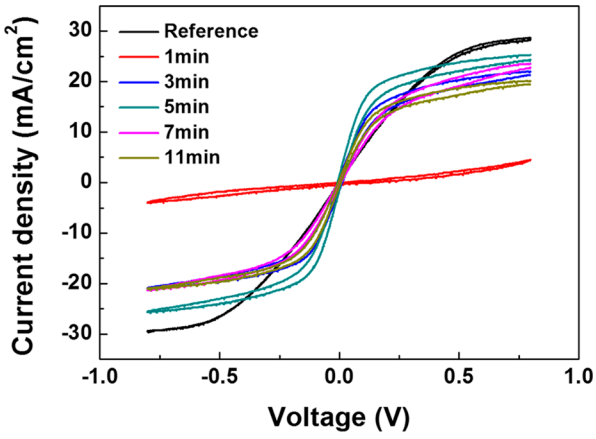

Figure 6. Cyclic voltammogram of a symmetrical cell with Pt-coated and SiNW/C counter electrodes, at a scan rate of 100 mV/s.

chemical behavior of the symmetric cells at a scan rate of 100 mV/s. All the counter electrodes except those with a 1 min carbon deposition sample showed the proper catalytic effect for I_3^- reduction. Even though the Pt-coated symmetrical cell showed the highest current density, 3−11 min carbon-deposited SiNW samples showed comparable catalytic abilities. Among the SiNW/C samples, the sample with a 5 min carbon coating showed the best current density, and this result was in agreement with that of the EIS analysis.

The $J-V$ curves of each counter electrode are shown in Figure 7, and the photovoltaic performances of these cells are listed in Table 3. The Pt-coated counter electrode cell showed a J_{sc} of 17.96 mA/cm^2, a V_{oc} of 0.81 V, and an FF of 67.03 with an efficiency of 9.75%. As shown by the CV analysis, because of the low current density, the J_{sc} value of the 5 min carbon-

dx.doi.org/10.1021/am504469y | ACS Appl. Mater. Interfaces 2014, 6, 18788−18794

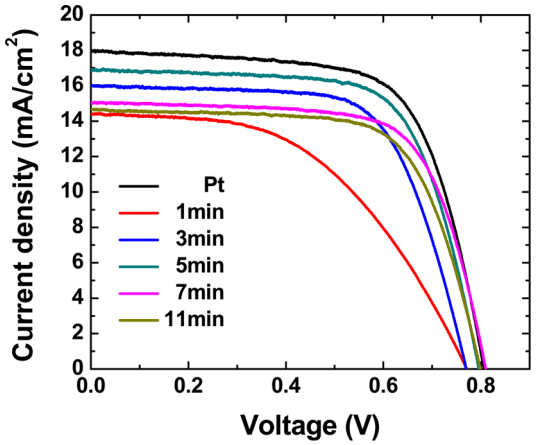

Figure 7. Photocurrent–voltage curves of DSSCs fabricated using different counter electrodes under AM 1.5G illumination.

Table 3. Photovoltaic Performances of Pt and SiNW/C Counter Electrodes

counter electrode	J_{sc} (mA/cm^2)	V_{oc} (V)	FF (%)	η (%)
Pt (reference)	17.96	0.810	67.03	9.75
1 min	14.60	0.778	50.27	5.71
3 min	16.02	0.777	66.12	8.23
5 min	16.91	0.802	67.98	9.22
7 min	15.54	0.818	68.66	8.73
11 min	15.60	0.804	68.01	8.53

deposited SiNW sample was lower (16.91 mA/cm^2) than that of the Pt-coated cell. However, other parameters showed a V_{oc} of 0.802 V and an FF of 67.89%. These values were comparable with that of the Pt-coated sample. The conversion efficiency of the best performing sample was 9.22%. In detail, FF values are almost the same for samples by Pt and carbon-coated SiNW except for the 1 min reacted sample. As the reaction time changes, V_{oc} values were increased as internal conductances of the counter electrodes are increased. A 3 min treated sample showed almost the same conductance (see Figure S5 of the Supporting Information) as the sample with a longer reaction time; its V_{oc} is only 0.777 V, which is close to the performance of the 1 min coated sample. This could be from possible uneven coating by a short time coating. J_{sc} shows different behaviors as we mentioned above. The photocurrent densities increase as the numbers of active catalytic sites increase because of the presence of more carbons. After using the optimal condition for 5 min, the extra carbons are not used for an increasing number of catalytic sites because it may cause surface area and porosity to decrease.

The stability test of DSSCs based on SiNW/C counter electrodes was implemented for 10 days as shown in Figure 8. The devices were stored in ambient air. While the efficiency, J_{sc}, and FF for the first 2 days decreased and then were kept almost constant, the V_{oc} continuously increased for the test period. After 10 days, the parameters of the efficiency, J_{sc}, V_{oc}, and FF retained 94, 94, 107, and 94% of their initial values, respectively. Prolonged stability under continuous illumination is shown in Figure S6 of the Supporting Information.

CONCLUSIONS

In summary, vertically aligned SiNW/C were fabricated using the electroless metal-assisted method. Subsequently, carbon coating with chemical vapor deposition was performed in the presence of a mixture of H_2 and CH_4. The amount of carbon deposited onto the SiNW surface was controlled by adjusting the reaction time from 1 to 11 min. We confirmed that the

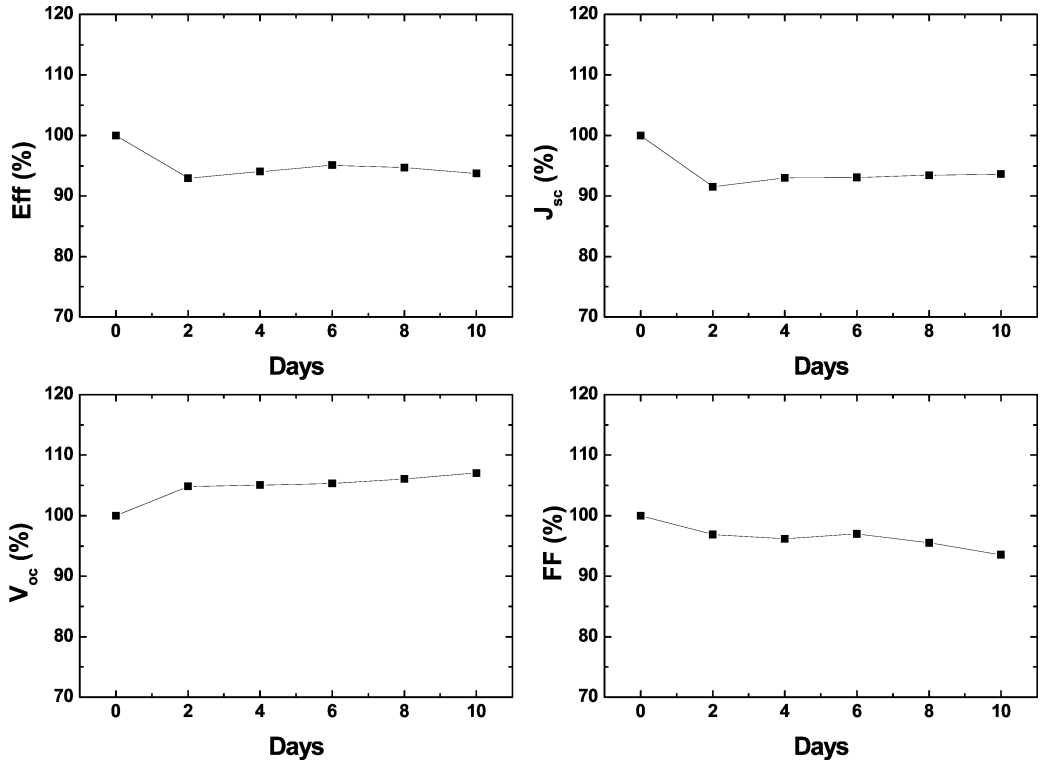

Figure 8. Long-term stability test for DSSCs based on carbon-coated SiNW counter electrodes.

SiNW/C helped to catalyze the reduction of I^-/I_3^- by using cyclic voltammetry and electrochemical impedance spectroscopy and subsequently employed them as counter electrodes in DSSCs. We obtained the highest power conversion efficiency of 9.22% with those 5 min SiNW/C, which had reacted for 5 min. This outcome was comparable to those of the Pt-based DSSCs (9.75%).

■ ASSOCIATED CONTENT

Supporting Information

Photograph of the DSSC based on the SiNW/C counter electrode, EDS spectrum of SiNW/C, EIS spectra of DSSCs based on Pt and each SiNW/C counter electrode, cyclic voltammograms of Pt and each SiNW/C sample recorded with the three-electrode setup, through-plane conductance data of each SiNW/C sample over the potential range from −0.1 to 0.1 V, and stability test of DSSCs fabricated with Pt and SiNW/C counter electrodes over 2 h. This material is available free of charge via the Internet at http://pubs.acs.org.

■ AUTHOR INFORMATION

Corresponding Authors

*Telephone: +82 2 450 0440. E-mail: yjun@konkuk.ac.kr.
*Telephone: +82 2 3290 3275. E-mail: donghwan@korea.ac.kr.

Author Contributions

J.K. and J.L. contributed equally to this work.

Notes

The authors declare no competing financial interest.

■ ACKNOWLEDGMENTS

This work was supported by a Korea Institute of Energy Technology Evaluation and Planning (KETEP) grant funded by the Korea government Ministry of Trade, Industry and Energy (20124030200120, 20123010010070, and 20133030000140).

■ REFERENCES

(1) Um, H. D.; Park, K. T.; Jung, J. Y.; Li, X.; Zhou, K.; Jee, S. W.; Lee, J. H. Incorporation of a Self-Aligned Selective Emitter to Realize Highly Efficient (12.8%) Si Nanowire Solar Cells. *Nanoscale* **2014**, *6*, 5193−5199.
(2) He, L.; Jiang, C.; Wang, H.; Lai, D.; Rusli. Si Nanowires Organic Semiconductor Hybrid Heterojunction Solar Cells toward 10% Efficiency. *ACS Appl. Mater. Interfaces* **2012**, *4*, 1704−1708.
(3) Syu, H. J.; Shiu, S. C.; Hung, Y. J.; Hsueh, C. C.; Lin, T. C.; Subramani, T.; Lee, S. L.; Lin, C. F. Influences of Silicon Nanowire Morphology on its Electro-Optical Properties and Applications for Hybrid Solar Cells. *Prog. Photovoltaics* **2013**, *21*, 1400−1410.
(4) Soci, C.; Zhang, A.; Xiang, B.; Dayeh, S. A.; Aplin, D. P. R.; Park, J.; Bao, X. Y.; Lo, Y. H.; Wang, D. Zno Nanowire UV Photodetectors with High Internal Gain. *Nano Lett.* **2007**, *7*, 1003−1009.
(5) Kim, D.; Kim, Y. K.; Park, S. C.; Ha, J. S.; Huh, J.; Na, J.; Kim, G. T. Photoconductance of Aligned SnO_2 Nanowire Field Effect Transistors. *Appl. Phys. Lett.* **2009**, *95*, 143107.
(6) De Luna Bugallo, A.; Tchernycheva, M.; Jacopin, G.; Rigutti, L.; Henri Julien, F.; Chou, S. T.; Lin, Y. T.; Tseng, P. H.; Tu, L. W. Visible-Blind Photodetector Based on p-i-n Junction GaN Nanowire Ensembles. *Nanotechnology* **2010**, *21*, 1−5.
(7) Yan, C.; Wang, J.; Wang, X.; Kang, W.; Cui, M.; Foo, C. Y.; Lee, P. S. An Intrinsically Stretchable Nanowire Photodetector with a Fully Embedded Structure. *Adv. Mater.* **2014**, *26*, 943−950.
(8) Cui, Y.; Zhong, Z.; Wang, D.; Wang, W. U.; Lieber, C. M. High Performance Silicon Nanowire Field Effect Transistors. *Nano Lett.* **2003**, *3*, 149−152.
(9) Wang, Y.; Chi, J.; Banerjee, K.; Grützmacher, D.; SchäPers, T.; Lu, J. G. Field Effect Transistor Based on Single Crystalline InSb Nanowire. *J. Mater. Chem.* **2011**, *21*, 2459−2462.
(10) Larrieu, G.; Han, X. L. Vertical Nanowire Array-Based Field Effect Transistors for Ultimate Scaling. *Nanoscale* **2013**, *5*, 2437−2441.
(11) Lee, J. H.; Kim, B. S.; Choi, S. H.; Jang, Y.; Hwang, S. W.; Whang, D. A Facile Route to Si Nanowire Gate-All-Around Field Effect Transistors with a Steep Subthreshold Slope. *Nanoscale* **2013**, *5*, 8968−8972.
(12) Chan, C. K.; Peng, H.; Liu, G.; McIlwrath, K.; Zhang, X. F.; Huggins, R. A.; Cui, Y. High-Performance Lithium Battery Anodes Using Silicon Nanowires. *Nat. Nanotechnol.* **2008**, *3*, 31−35.
(13) Chan, C. K.; Patel, R. N.; O'Connell, M. J.; Korgel, B. A.; Cui, Y. Solution-Grown Silicon Nanowires for Lithium-Ion Battery Anodes. *ACS Nano* **2010**, *4*, 1443−1450.
(14) Yan, J.; Sumboja, A.; Khoo, E.; Lee, P. S. V_2O_5 Loaded on SnO_2 Nanowires for High-Rate Li Lon Batteries. *Adv. Mater.* **2011**, *23*, 746−750.
(15) Hayden, O.; Greytak, A. B.; Bell, D. C. Core-Shell Nanowire Light-Emitting Diodes. *Adv. Mater.* **2005**, *17*, 701−704.
(16) Zimmler, M. A.; Voss, T.; Ronning, C.; Capasso, F. Exciton-Related Electroluminescence from ZnO Nanowire Light-Emitting Diodes. *Appl. Phys. Lett.* **2009**, *94*, 241120.
(17) Chen, C. Y.; Zhu, G.; Hu, Y.; Yu, J. W.; Song, J.; Cheng, K. Y.; Peng, L. H.; Chou, L. J.; Wang, Z. L. Gallium Nitride Nanowire Based Nanogenerators and Light-Emitting Diodes. *ACS Nano* **2012**, *6*, 5687−5692.
(18) Xia, X.; Tu, J.; Zhang, Y.; Wang, X.; Gu, C.; Zhao, X. B.; Fan, H. J. High-Quality Metal Oxide Core/Shell Nanowire Arrays on Conductive Substrates for Electrochemical Energy Storage. *ACS Nano* **2012**, *6*, 5531−5538.
(19) Sun, Z.; Ai, W.; Liu, J.; Qi, X.; Wang, Y.; Zhu, J.; Zhang, H.; Yu, T. Facile Fabrication of Hierarchical $ZnCo_2O_4$/NiO Core/Shell Nanowire Arrays with Improved Lithium-Ion Battery Performance. *Nanoscale* **2014**, *6*, 6563−6568.
(20) Li, G. R.; Wang, F.; Song, J.; Xiong, F. Y.; Gao, X. P. Tin-Conductive Carbon Black Composite as Counter Electrode for Dye-Sensitized Solar Cells. *Electrochim. Acta* **2012**, *65*, 216−220.
(21) Lee, W. J.; Ramasamy, E.; Lee, D. Y.; Song, J. S. Efficient Dye-Sensitized Solar Cells with Catalytic Multiwall Carbon Nanotube Counter Electrodes. *ACS Appl. Mater. Interfaces* **2009**, *1*, 1145−1149.
(22) Siriroj, S.; Pimanpang, S.; Towannang, M.; Maiaugree, W.; Phumying, S.; Jarernboon, W.; Amornkitbamrung, V. High Performance Dye-Sensitized Solar Cell Based on Hydrothermally Deposited Multiwall Carbon Nanotube Counter Electrode. *Appl. Phys. Lett.* **2012**, *100*, 1−4.
(23) Kavan, L.; Yum, J. H.; Nazeeruddin, M. K.; Grätzel, M. Graphene Nanoplatelet Cathode for Co(III)/(II) Mediated Dye-Sensitized Solar Cells. *ACS Nano* **2011**, *5*, 9171−9178.
(24) Ju, M. J.; Kim, J. C.; Choi, H. J.; Choi, I. T.; Kim, S. G.; Lim, K.; Ko, J.; Lee, J. J.; Jeon, I. Y.; Baek, J. B.; Kim, H. K. N-Doped Graphene Nanoplatelets as Superior Metal-Free Counter Electrodes for Organic Dye-Sensitized Solar Cells. *ACS Nano* **2013**, *7*, 5243−5250.
(25) Erwin, W. R.; Oakes, L.; Chatterjee, S.; Zarick, H. F.; Pint, C. L.; Bardhan, R. Engineered Porous Silicon Counter Electrodes for High Efficiency Dye-Sensitized Solar Cells. *ACS Appl. Mater. Interfaces* **2014**, *6*, 9904−9910.
(26) Wu, W.-Q.; Feng, H.-L.; Rao, H.-S.; Xu, Y.-F.; Kuang, D.-B.; Su, C.-Y. Maximizing Omnidirectional Light Harvesting in Metal Oxide Hyperbranched Array Architectures. *Nat. Commun.* **2014**, *5*, 1−9.
(27) Wu, W.-Q.; Xu, Y.-F.; Rao, H.-S.; Su, C.-Y.; Kuang, D.-B. Multistack Integration of Three-Dimensional Hyperbranched Anatase Titania Architectures for High-Efficiency Dye-Sensitized Solar Cells. *J. Am. Chem. Soc.* **2014**, *136*, 6437−6445.
(28) Wu, W.-Q.; Xu, Y.-F.; Su, C.-Y.; Kuang, D.-B. Ultra-Long Anatase TiO_2 Nanowire Arrays With Multi-Layered Configuration On FTO Glass for High-Efficiency Dye-Sensitized Solar Cells. *Energy Environ. Sci.* **2014**, *7*, 644−649.

(29) Cho, Y. J.; Kim, H. S.; Im, H.; Myung, Y.; Jung, G. B.; Lee, C. W.; Park, J.; Park, M. H.; Cho, J.; Kang, H. S. Nitrogen-Doped Graphitic Layers Deposited on Silicon Nanowires for Efficient Lithium-Ion Battery Anodes. *J. Phys. Chem. C* **2011**, *115*, 9451−9457.
(30) Yang, Y.; Ren, J. G.; Wang, X.; Chui, Y. S.; Wu, Q. H.; Chen, X.; Zhang, W. Graphene Encapsulated and SiC Reinforced Silicon Nanowires as an Anode Material for Lithium Ion Batteries. *Nanoscale* **2013**, *5*, 8689−8694.
(31) Chen, C. Y.; Wu, C. S.; Chou, C. J.; Yen, T. J. Morphological Control of Single-Crystalline Silicon Nanowire Arrays near Room Temperature. *Adv. Mater.* **2008**, *20*, 3811−3815.
(32) Zhang, M. L.; Peng, K. Q.; Fan, X.; Jie, J. S.; Zhang, R. Q.; Lee, S. T.; Wong, N. B. Preparation of Large-Area Uniform Silicon Nanowires Arrays through Metal-Assisted Chemical Etching. *J. Phys. Chem. C* **2008**, *112*, 4444−4450.
(33) Shalagina, A. E.; Ismagilov, Z. R.; Podyacheva, O. Y.; Kvon, R. I.; Ushakov, V. A. Synthesis of Nitrogen-Containing Carbon Nanofibers by Catalytic Decomposition of Ethylene/Ammonia Mixture. *Carbon* **2007**, *45*, 1808−1820.
(34) Piscanec, S.; Cantoro, M.; Ferrari, A. C.; Zapien, J. A.; Lifshitz, Y.; Lee, S. T.; Hofmann, S.; Robertson, J. Raman Spectroscopy of Silicon Nanowires. *Phys. Rev. B* **2003**, *68*, 2413121−2413124.
(35) Nii, H.; Sumiyama, Y.; Nakagawa, H.; Kunishige, A. Influence of Diameter on the Raman Spectra of Multi-Walled Carbon Nanotubes. *Appl. Phys. Express* **2008**, *1*, 0640051−0640053.
(36) Wang, G.; Xing, W.; Zhuo, S. Nitrogen-Doped Graphene as Low-Cost Counter Electrode for High-Efficiency Dye-Sensitized Solar Cells. *Electrochim. Acta* **2013**, *92*, 269−275.
(37) Cruz, R.; Araújo, J. P.; Andrade, L.; Mendes, A. Transparent Graphene-Based Counter-Electrodes for Iodide/Triiodide Mediated Dye-Sensitized Solar Cells. *J. Mater. Chem. A* **2014**, *2*, 2028−2032.
(38) Akbar, Z. A.; Lee, J. S.; Kang, J.; Joh, H. I.; Lee, S.; Jang, S. Y. FTO-Free Counter Electrodes for Dye-Sensitized Solar Cells Using Carbon Nanosheets Synthesised from a Polymeric Carbon Source. *Phys. Chem. Chem. Phys.* **2014**, *16*, 17595−17602.
(39) Lin, J. Y.; Liao, J. H.; Chou, S. W. Cathodic Electrodeposition of Highly Porous Cobalt Sulfide Counter Electrodes for Dye-Sensitized Solar Cells. *Electrochim. Acta* **2011**, *56*, 8818−8826.
(40) Kavan, L.; Yum, J. H.; Grätzel, M. Optically Transparent Cathode for Dye-Sensitized Solar Cells Based on Graphene Nanoplatelets. *ACS Nano* **2011**, *5*, 165−172.
(41) Dao, V. D.; Choi, H. S. An Optimum Morphology of Platinum Nanoparticles with Excellent Electrocatalytic Activity for a Highly Efficient Dye-Sensitized Solar Cell. *Electrochim. Acta* **2013**, *93*, 287−292.
(42) Lim, J.; Ryu, S. Y.; Kim, J.; Jun, Y. A Study of TiO_2/Carbon Black Composition as Counter Electrode Materials for Dye-Sensitized Solar Cells. *Nanoscale Res. Lett.* **2013**, *8*, 1−5.
(43) Jo, Y.; Cheon, J. Y.; Yu, J.; Jeong, H. Y.; Han, C. H.; Jun, Y.; Joo, S. H. Highly Interconnected Ordered Mesoporous Carbon-Carbon Nanotube Nanocomposites: Pt-Free, Highly Efficient, and Durable Counter Electrodes for Dye-Sensitized Solar Cells. *Chem. Commun.* **2012**, *48*, 8057−8059.
(44) Li, L. L.; Chang, C. W.; Wu, H. H.; Shiu, J. W.; Wu, P. T.; Wei-Guang Diau, E. Morphological Control of Platinum Nanostructures for Highly Efficient Dye-Sensitized Solar Cells. *J. Mater. Chem.* **2012**, *22*, 6267−6273.
(45) Yeh, M. H.; Lin, L. Y.; Sun, C. L.; Leu, Y. A.; Tsai, J. T.; Yeh, C. Y.; Vittal, R.; Ho, K. C. Multiwalled Carbon Nanotube@Reduced Graphene Oxide Nanoribbon as the Counter Electrode for Dye-Sensitized Solar Cells. *J. Phys. Chem. C* **2014**, *118*, 16626−16634.